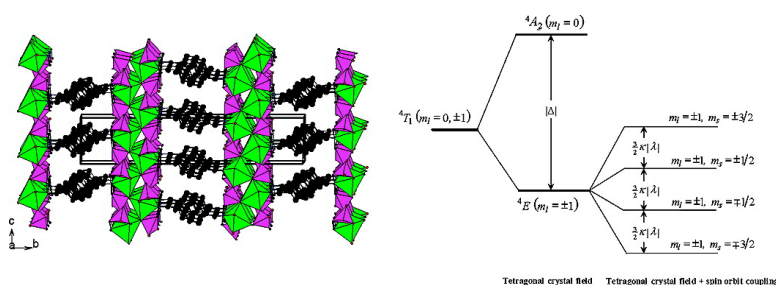Article

A Highly Anisotropic Cobalt(II)-Based Single-Chain Magnet: Exploration of Spin Canting in an Antiferromagnetic Array

Andrei V. Palii, Oleg S. Reu, Sergei M. Ostrovsky, Sophia I. Klokishner, Boris S. Tsukerblat,
Zhong-Ming Sun, Jiang-Gao Mao, Andrey V. Prosvirin, Han-Hua Zhao, and Kim R. Dunbar

More About This Article

Additional resources and features associated with this article are available within the HTML version:

- Supporting Information
- Links to the 1 articles that cite this article, as of the time of this article download
- Access to high resolution figures
- Links to articles and content related to this article
- Copyright permission to reproduce figures and/or text from this article

View the Full Text HTML

A Highly Anisotropic Cobalt(II)-Based Single-Chain Magnet: Exploration of Spin Canting in an Antiferromagnetic Array

Andrei V. Palii,*,† Oleg S. Reu,† Sergei M. Ostrovsky,† Sophia I. Klokishner,†
Boris S. Tsukerblat,*,‡ Zhong-Ming Sun,§ Jiang-Gao Mao,§ Andrey V. Prosvirin,‖
Han-Hua Zhao,‖ and Kim R. Dunbar*,‖

*Institute of Applied Physics of the Academy of Sciences of Moldova, Academy str. 5,
Chisinau MD-2068, Moldova, Chemistry Department, Ben-Gurion University of the Negev,
Beer-Sheva 84105, Israel, State Key Laboratory of Structural Chemistry, Fujian Institute of
Research on the Structure of Matter, Chinese Academy of Sciences, Fuzhou 350002, People's
Republic of China, and Department of Chemistry, Texas A&M University,
P.O. Box 30012, College Station, Texas 77843-3012*

Received June 30, 2008; E-mail: andrew.palii@uv.es; tsuker@bgu.ac.il; dunbar@mail.chem.tamu.edu

Abstract: In this article we report for the first time experimental details concerning the synthesis and full characterization (including the single-crystal X-ray structure) of the spin-canted zigzag-chain compound $[Co(H_2L)(H_2O)]_\infty$ [L = 4-Me-C_6H_4-$CH_2N(CPO_3H_2)_2$], which contains antiferromagnetically coupled, highly magnetically anisotropic Co(II) ions with unquenched orbital angular momenta, and we also propose a new model to explain the single-chain magnet behavior of this compound. The model takes into account (1) the tetragonal crystal field and the spin—orbit interaction acting on each Co(II) ion, (2) the antiferromagnetic Heisenberg exchange between neighboring Co(II) ions, and (3) the tilting of the tetragonal axes of the neighboring Co units in the zigzag structure. We show that the tilting of the anisotropy axes gives rise to spin canting and consequently to a nonvanishing magnetization for the compound. In the case of a strong tetragonal field that stabilizes the orbital doublet of Co(II), the effective pseudo-spin-$^1/_2$ Hamiltonian describing the interaction between the Co ions in their ground Kramers doublet states is shown to be of the Ising type. An analytical expression for the static magnetic susceptibility of the infinite spin-canted chain is obtained. The model provides an excellent fit to the experimental data on both the static and dynamic magnetic properties of the chain.

Introduction

One-dimensional (1D) systems that exhibit magnetic bistability, which are commonly called single-chain magnets (SCMs), are of great interest because of their unusual physical properties and their potential importance for high-density data storage and quantum-computing applications.[1,2] During the past few years, this branch of molecular magnetism dealing with 1D magnets has become an area of intense research activity.[3−16] In contrast

to single-molecule magnets,[1,2] the slow relaxation of magnetization in SCMs is due to the exchange interaction between rapidly relaxing units. The theoretical background for the description of SCM behavior is provided by Glauber's stochastic approach.[17] Glauber predicted the presence of slow relaxation of magnetization in a chain composed of ferromagnetically coupled spins that can be described by the Ising Hamiltonian:

† Academy of Sciences of Moldova.
‡ Ben-Gurion University of the Negev.
§ Fujian Institute of Research on the Structure of Matter.
‖ Texas A&M University.

(1) Gatteschi, D.; Sessoli, R.; Villain, J. *Molecular Nanomagnets*; Oxford University Press: Oxford, U.K., 2006.
(2) Gatteschi, D.; Sessoli, R. *Angew. Chem., Int. Ed.* **2003**, *42*, 268.
(3) Caneschi, A.; Gatteschi, D.; Lalioti, N.; Sangregorio, C.; Sessoli, R.; Venturi, G.; Vindigni, A.; Rettori, A.; Pini, M. G.; Novak, M. A. *Angew. Chem., Int. Ed.* **2001**, *40*, 1760.
(4) Caneschi, A.; Gatteschi, D.; Lalioti, N.; Sessoli, R.; Sorace, L.; Tangoulis, V.; Vindigni, A. *Chem.—Eur. J.* **2002**, *8*, 286.
(5) Caneschi, A.; Gatteschi, D.; Lalioti, N.; Sangregorio, C.; Sessoli, R.; Venturi, G.; Vindigni, A.; Rettori, A.; Pini, M. G.; Novak, M. A. *Europhys. Lett.* **2002**, *58*, 771.
(6) Clérac, R.; Miyasaka, H.; Yamashita, M.; Coulon, C. *J. Am. Chem. Soc.* **2002**, *124*, 12837.
(7) Lescouëzec, R.; Vaissermann, J.; Ruiz-Perez, C.; Lloret, F.; Carrasco, R.; Julve, M.; Verdaguer, M.; Dromzee, Y.; Gatteschi, D.; Wernsdorfer, W. *Angew. Chem., Int. Ed.* **2003**, *42*, 1483.

(8) Miyasaka, H.; Clérac, R.; Mizushima, K.; Sugiura, K.; Yamashita, M.; Wernsdorfer, W.; Coulon, C. *Inorg. Chem.* **2003**, *42*, 8203.
(9) Toma, L. M.; Lescouëzec, R.; Lloret, F.; Julve, M.; Vaissermann, J.; Verdaguer, M. *Chem. Commun.* **2003**, 1850.
(10) Costes, J.-P.; Clemente-Juan, J. M.; Dahan, F.; Milon, J. *Inorg. Chem.* **2004**, *43*, 8200.
(11) Ferbinteanu, M.; Miyasaka, H.; Wernsdorfer, W.; Nakata, K.; Sugiura, K.; Yamashita, M.; Coulon, C.; Clérac, R. *J. Am. Chem. Soc.* **2005**, *127*, 3090.
(12) Zheng, Y.-Z.; Tong, M.-L.; Zhang, W.-X.; Chen, X.-M. *Angew. Chem., Int. Ed.* **2006**, *45*, 6310.
(13) Liu, T. F.; Fu, D.; Gao, S.; Zhang, Y.-Z.; Sun, H.-L.; Su, G.; Liu, Y.-J. *J. Am. Chem. Soc.* **2003**, *125*, 13976.
(14) Sun, Z.-M.; Prosvirin, A. V.; Zhao, H.-H.; Mao, J.-G.; Dunbar, K. R. *J. Appl. Phys.* **2005**, *97*, 10B305.
(15) Liu, X.-T.; Wang, X.-Y.; Zhang, W.-X.; Cui, P.; Gao, S. *Adv. Mater.* **2006**, *18*, 2852.
(16) Bernot, K.; Luzon, J.; Sessoli, R.; Vindigni, A.; Thion, J.; Richeter, S.; Leclercq, D.; Larionova, J.; van der Lee, A. *J. Am. Chem. Soc.* **2008**, *130*, 1619.
(17) Glauber, R. J. *J. Math. Phys.* **1963**, *4*, 294.

$$\hat{H}_{ex} = -2J\sum_{i<j} \hat{\tau}_Z(i)\hat{\tau}_Z(j) \qquad (1)$$

where $\hat{\tau}_Z$ is the operator for the Z component of the spin or pseudospin and J is the coupling constant. In Glauber's theory, the thermal variation of the relaxation time τ is described by the Arrhenius law

$$\tau(T) = \tau_0 \exp\left(\frac{\Delta_b}{k_B T}\right) \qquad (2)$$

in which Δ_b, the barrier to reverse the magnetization direction, represents the energy loss in one spin flip-flop process, that is,

$$\Delta_b = 2J \qquad (3)$$

An Ising spin chain can behave as an SCM if the constituent magnetic units are coupled in such a way that their magnetic moments do not cancel. In the majority of known SCMs, this condition is satisfied by virtue of either ferromagnetic interactions between spins or alternation of different antiferromagnetically coupled spins. Recently, several examples of SCMs containing a single type of spin center (homospin systems) have been reported: chains composed of ferromagnetically coupled Co(II) ions have been considered,[12,13] and additionally, the unusual SCMs containing antiferromagnetically coupled Co(II),[14] Mn(III),[15] and Ni(II)[16] ions have been discovered. In these latter compounds, the uncompensated magnetic moment was shown to appear as a result of noncollinear spin structure (spin canting). The first well-documented example of this unusual type of SCM with antiferromagnetic exchange was reported in our recent article[14] concerning the cobalt(II) diphosphonate material $[Co(H_2L)(H_2O)]_\infty$ [L = 4-Me-C_6H_4-CH_2N-$(CPO_3H_2)_2$], in which the Co(II) ions are linked through bridging phosphonate oxygen atoms to create a 1D chain of corner-sharing octahedra that propagates in a zigzag fashion.

An initial attempt to understand the unusual magnetic behavior of $[Co(H_2L)(H_2O)]_\infty$ was undertaken in our recent article,[18] where we deduced the effective pseudospin-$\frac{1}{2}$ Hamiltonian for a chain and demonstrated that an uncompensated magnetic moment at low temperatures is a result of spin canting. However, the model in that earlier work[18] was based on the mean-field approach, which allows a qualitative explanation of all of the characteristic features of the observed phenomena but fails in the quantitative description of the magnetic susceptibility. The aim of this article is to present a quantum-mechanical approach for describing the SCM behavior and the spin-canting phenomenon in this system. We present a relatively simple model that incorporates the main factors responsible for the SCM behavior of the compound, namely, the strong uniaxial magnetic anisotropy arising from the tetragonal ligand fields acting on the Co(II) ions, the spin−orbit interaction, the aniferromagnetic exchange, and the topology of the chain. The combination of these factors gives rise to a canted spin structure and subsequently to an uncompensated magnetic moment. Finally, we demonstrate that the model agrees perfectly with the experimental data on the static and dynamic susceptibility behavior of $[Co(H_2L)(H_2O)]_\infty$ compound. We also report for the first time experimental details of the synthesis and full characterization of the compound, since the previous reports

Scheme 1. Illustration of the Hydrothermal Reaction To Form $[Co(H_2L)(H_2O)]_\infty$, Showing the Basic Connectivity Pattern of the Ligands To Form a 1D Zigzag Motif
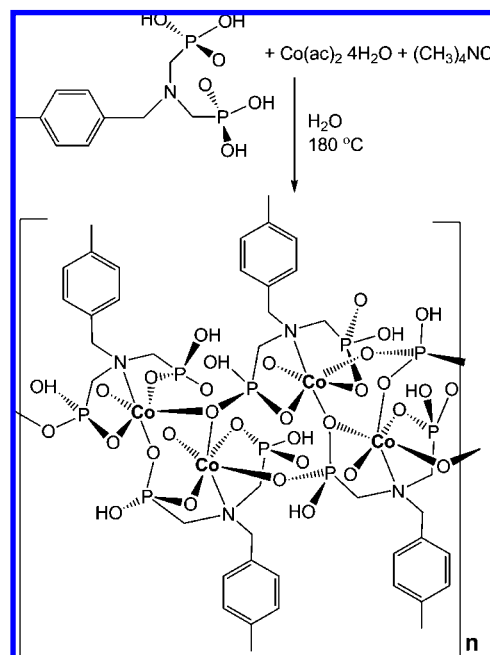
contained information solely about the magnetic properties and a preliminary model to account for the magnetic behavior.[14,18]

Experimental Section

Materials and Methods. All of the chemicals and solvents were of reagent-grade quality and used as received. Elemental analyses were performed on a German Elementary Vario EL III instrument. Thermogravimetric analysis was carried out with a TGA/SBTA851 unit at a heating rate of 15 °C/min under a nitrogen atmosphere. Infrared spectra were recorded on a Magna 750 FT-IR spectrometer as KBr pellets over the range 4000−400 cm^{-1}. XRD powder patterns were collected on a Philips X'Pert-MPD diffractometer using graphite-monochromatized Cu Kα radiation in the range $2\theta = 5-70°$ with a step size of 0.02° and a count time of 3 s per step.

Synthesis of the Diphosphonate H₄L Ligand. The diphosphonic acid 4-Me-C_6H_4-$CH_2N(CH_2PO_3H_2)_2$ (H₄L) was synthesized by a Mannich-type reaction according to a literature procedure.[19]

Synthesis of $[Co(H_2L)(H_2O)]_\infty$. A mixture of 0.5 mmol of H₄L, 0.5 mmol of $Co(ac)_2\cdot 4H_2O$, 3 mL of 10% tetramethylammonium chloride aqueous solution, and 10 mL of deionized water was sealed into a bomb equipped with a Teflon liner (25 mL) and heated at 180 °C for 4 days. Pink brick-shaped crystals of $Co(H_2L)(H_2O)$ were obtained in 60% yield based on cobalt. The initial and final pH values were 3.5 and 3.0, respectively. Elemental analysis for $Co(H_2L)(H_2O)$, $C_{10}H_{17}NO_7P_2Co$: C, 30.95; H, 4.25; N, 3.42. Calcd: C, 31.27; H, 4.46; N, 3.65. IR data (KBr pellet, cm^{-1}): 3535 (s), 3352 (m), 3263 (m), 2912 (m), 2343(br), 1658 (m), 1454 (w), 1421 (w), 1174 (s), 1139 (s), 919 (s), 804 (m), 750 (w), 457 (w). The purity of the title compound was also confirmed by its X-ray powder pattern. A schematic drawing of the reaction is provided in Scheme 1.

Single-Crystal X-ray Structural Determination. A single crystal of the title compound was mounted on a Bruker Smart CCD using Mo Kα radiation ($\lambda = 0.71069$ Å) equipped with a graphite monochromator at room temperature. Intensity data were collected using a narrow-frame method with 0.3° per frame in 2θ at 293 K. An absorption correction was performed with the SADABS

(18) Palii, A. V.; Ostrovsky, S. M.; Klokishner, S. I.; Reu, O. S.; Sun, Z.-M.; Prosvirin, A. V.; Zhao, H.-H.; Mao, J.-G.; Dunbar, K. R. *J. Phys. Chem. A* **2006**, *110*, 14003.

(19) Sun, Z.-M.; Yang, B.-P.; Sun, Y.-Q.; Mao, J.-G.; Clearfield, A. *J. Solid State Chem.* **2003**, *176*, 62.

Table 1. Crystal and Refinement Parameters for [Co(H$_2$L)(H$_2$O)]$_\infty$[a]

empirical formula	C$_{10}$H$_{17}$CoNO$_7$P$_2$
M	384.12
crystal system	monoclinic
space group	P2$_1$/c (No. 14)
T (K)	298(1)
a (Å)	8.3540(13)
b (Å)	29.211(4)
c (Å)	6.2171(9)
β (deg)	110.621(3)
V (Å^3)	1420.0(4)
Z	4
D$_c$ (g cm^{-3})	1.797
μ(Mo Kα) (mm^{-1})	1.466
GOF	1.060
R1, wR2 [I > 2σ(I)]^a	0.0702, 0.1079
R1, wR2 (all data)^a	0.1382, 0.1325

^{a} R1 = $\sum\|\|F_o\| - \|F_c\|\|/\sum\|F_o\|$; wR2 = $\{\sum w[(F_o)^2 - (F_c)^2]^2/\sum w[(F_o)^2]^2\}^{1/2}$.

Table 2. Selected Bond Distances and Angles for [Co(H$_2$L)(H$_2$O)]$_\infty$[a]

Bond Distances (Å)			
Co(1)−O(22)#1	2.035(5)	Co(1)−O(1W)	2.098(5)
Co(1)−O(13)	2.134(5)	Co(1)−O(23)#2	2.139(5)
Co(1)−O(23)	2.176(5)	Co(1)−N(1)	2.282(6)
P(1)−O(12)	1.497(5)	P(1)−O(13)	1.519(5)
P(1)−O(11)	1.581(5)	P(2)−O(22)	1.489(5)
P(2)−O(23)	1.528(5)	P(2)−O(21)	1.561(5)

Bond Angles (deg)			
O(22)#1−Co(1)−O(1W)	90.1(2)	O(22)#1−Co(1)−O(13)	93.7(2)
O(1W)−Co(1)−O(13)	175.5(2)	O(22)#1−Co(1)−O(23)#2	84.98(19)
O(1W)−Co(1)−O(23)#2	90.8(2)	O(13)−Co(1)−O(23)#2	91.87(19)
O(22)#1−Co(1)−O(23)	166.2(2)	O(1W)−Co(1)−O(23)	84.14(19)
O(13)−Co(1)−O(23)	91.58(19)	O(23)#2−Co(1)−O(23)	107.63(13)
O(22)#1−Co(1)−N(1)	83.5(2)	O(1W)−Co(1)−N(1)	98.4(2)
O(13)−Co(1)−N(1)	79.7(2)	O(23)#2−Co(1)−N(1)	165.2(2)
O(23)−Co(1)−N(1)	84.90(19)	Co(1)#4−O(23)−Co(1)	122.1(2)

^{a} Symmetry transformations used to generate equivalent atoms: (#1) x, y, z − 1; (#2) x, −y + ^{3}/$_2$, z − ^{1}/$_2$.

program.[20] The structure was solved by direct methods and all of the non-hydrogen atoms were refined by full-matrix least-squares fitting on F^2 using the SHELXS program.[20] Hydrogen atoms were located at geometrically calculated positions and refined with isotropic thermal parameters. A summary of the crystallographic data is listed in Table 1. Selected bond distances and angles are provided in Table 2.

Discussion of the Structure. The cobalt(II) ion in [Co(H$_2$L)-(H$_2$O)]$_\infty$ is in a ligand environment consisting of a tridentate chelating diphosphonate ligand contributing one N and two O atoms, two phosphonate oxygen atoms, one from each of two adjacent Co(H$_2$L) chelating units, and a water molecule (Figure 1). The Co−N bond distance is 2.282(6) Å, and the Co−O distances are in the range 2.035(5)−2.176(5) Å. These distances are comparable to those reported for other cobalt(II) phosphonates.[21−27] The pentadentate diphosphonate ligand, which is doubly protonated (O11 and O21), acts as a tridentate ligand chelating to one Co(II) ion and as a bridge to independent Co(II) ions. The phosphonate group containing the P1 atom bears a −1 charge, and the ligand containing P2 is tridentate. The O23 atom is a μ_2 bridge, with a Co(1)−O(23)−Co1D bond angle of 122.1(2)°. This type of coordination mode is significantly different from that observed in the analogous Cd(HL)$_2$ chain, in which the diphosphonate anion is uninegative and the amine group is protonated. In that compound, the diphosphonate ligand is not involved in metal chelation.

The extended interactions in the structure involve Co(II) octahedra interconnected via corner-sharing oxygen atoms (O23) to form a 1D zigzag chain (Figure 2a). There are two types of intrachain Co$\cdots$Co separations: those involving cobalt(II) centers bridged by corner-sharing oxygen atoms [3.775(1) Å] and those involving a bridging phosphonate group [6.217(1) Å]. This type of 1D chain is different from the Cd(HL)$_2$ structure, in which all of the Cd(II) ions are spanned by Cd−O−P−O−Cd bridges. As in the case of Cd(HL)$_2$, however, neighboring 1D chains in [Co(H$_2$L)(H$_2$O)]$_\infty$ are involved in hydrogen bonds between phosphonate oxygen atoms to form an overall layered architecture in the *ac* plane, as depicted schematically in Figure 2(b). As the view of the chains in Figure 3 clearly shows, the Me-C$_6$H$_4$-CH$_2$− substituents on the phosphonate groups extend into the spaces between layers. The presence of these bulky groups prevents close approach of the chains, as attested by the fact that the nearest interchain Co$\cdots$Co distance is 8.108(2) Å, and serves to further stabilize the structure by making possible π−π interactions between neighboring layers. The distance between adjacent parallel ring centers is 3.633(7) Å.

An IR spectrum of [Co(H$_2$L)(H$_2$O)]$_\infty$ in the range 4000−400 cm^{-1} (not shown) was recorded in order to examine the water of hydration and the P−O−H groups. The absorption at 2912 cm^{-1} was attributed to a ν(N−H) mode. The broad, intense band at 3535 cm^{-1} was due to the O−H stretch of a hydrogen-bonded water molecule. A δ(H−O−H) bending mode was located at 1658 cm^{-1}. The set of features between 1200 and 900 cm^{-1} was assigned to stretching vibrations of the tetrahedral CPO$_3$ groups.

A TGA analysis under a nitrogen atmosphere (not shown) indicated that the compound is stable up to 235 °C, above which temperature it first loses the water of hydration and then releases one water molecule and a CH$_3$-C$_6$H$_4$-CH$_2$− moiety formed by condensation of the hydrogen phosphonate groups. The final residue at 1000 °C was a mixture of CoO and Co(PO$_3$)$_2$, as determined on the basis of X-ray powder diffraction data.

New Model and Magnetic Parameters. The crystallographic positions of neighboring Co(II) ions in the chain are inequivalent

(20) (a) Sheldrick, G. M. *Program SADABS*; University of Göttingen: Göttingen, Germany, 1995. (b) Sheldrick, G. M. *SHELXTL Crystallographic Software Package*, version 5.1; Bruker-AXS: Madison, WI, 1998.

(21) (a) Burkholder, E.; Golub, V.; O'Connor, C. J.; Zubieta, J. *Chem. Commun.* **2003**, 2128. (b) Burkholder, E.; Golub, V.; O'Connor, C. J.; Zubieta, J. *Inorg. Chem.* **2003**, *42*, 6729. (c) Finn, R. C.; Burkholder, E.; Zubieta, J. *Chem. Commun.* **2001**, 1852. (d) Finn, R. C.; Lam, R.; Greedan, J. E.; Zubieta, J. *Inorg. Chem.* **2001**, *40*, 3745. (e) Finn, R. C.; Zubieta, J. *Inorg. Chem.* **2001**, *40*, 2466.

(22) (a) Calin, N.; Sevov, S. C. *Inorg. Chem.* **2003**, *42*, 7304. (b) Distler, A.; Lohse, D. L.; Sevov, S. C. *J. Chem. Soc., Dalton Trans.* **1999**, 1805. (c) Dumas, E.; Sassoye, C.; Smith, K. D.; Sevov, S. C. *Inorg. Chem.* **2002**, *41*, 4029.

(23) (a) Yin, P.; Gao, S.; Zheng, L. M.; Wang, Z. M.; Xin, X. Q. *Chem. Commun.* **2003**, 1076. (b) Yin, P.; Gao, S.; Zheng, L. M.; Xin, X. Q. *Chem. Mater.* **2003**, *15*, 3233. (c) Zheng, L. M.; Gao, S.; Yin, P.; Xin, X.-Q. *Inorg. Chem.* **2004**, *43*, 2151. (d) Zheng, L. M.; Gao, S.; Song, H. H.; Decurtins, S.; Jacobson, A. J.; Xin, X.-Q. *Chem. Mater.* **2002**, *14*, 3143. (e) Yin, P.; Zheng, L. M.; Gao, S.; Xin, X. Q. *Chem. Commun.* **2001**, 2346.

(24) (a) Barthelet, K.; Nogues, M.; Riou, D.; Ferey, G. *Chem. Mater.* **2002**, *14*, 4910. (b) Serre, C.; Ferey, G. *Inorg. Chem.* **2001**, *40*, 5350. (c) Serre, C.; Ferey, G. *Inorg. Chem.* **1999**, *38*, 5370. (d) Gao, Q. M.; Guillou, N.; Nogues, M.; Cheetham, A. K.; Ferey, G. *Chem. Mater.* **1999**, *11*, 2937. (e) Serpaggi, F.; Ferey, G. *J. Mater. Chem.* **1998**, *8*, 2749.

(25) (a) Stock, N.; Bein, T. *Angew. Chem., Int. Ed.* **2004**, *43*, 749. (b) Fu, R. B.; Wu, X. T.; Hu, S. M.; Zhang, J. J.; Fu, Z. Y.; Du, W. X.; Xia, S. Q. *Eur. J. Inorg. Chem.* **2003**, 1798. (c) Bujoli-Doeuff, M.; Evain, M.; Janvier, P.; Massiot, D.; Clearfield, A.; Gan, Z. H.; Bujoli, B. *Inorg. Chem.* **2001**, *40*, 6694. (d) Odobel, F.; Bujoli, B.; Massiot, D. *Chem. Mater.* **2001**, *13*, 163. (e) Fu, R. B.; Hu, S. M.; Fu, Z. Y.; Zhang, J. J.; Wu, X. T. *New J. Chem.* **2003**, *27*, 230.

(26) Sun, Z.-M.; Mao, J.-G.; Sun, Y.-Q.; Zeng, H.-Y.; Clearfield, A. *New J. Chem.* **2003**, *27*, 1326.

(27) (a) Coulon, C.; Clérac, R.; Lecren, L.; Wernsdorfer, W.; Miyasaka, H. *Phys. Rev. B* **2004**, *69*, 132408. (b) Mito, M.; Shindo, N.; Tajiri, T.; Deguchi, H.; Takagi, S.; Miyasaka, H.; Yamashita, M.; Clérac, R.; Coulon, C. *J. Magn. Magn. Mater.* **2004**, *272−276*, 1118.
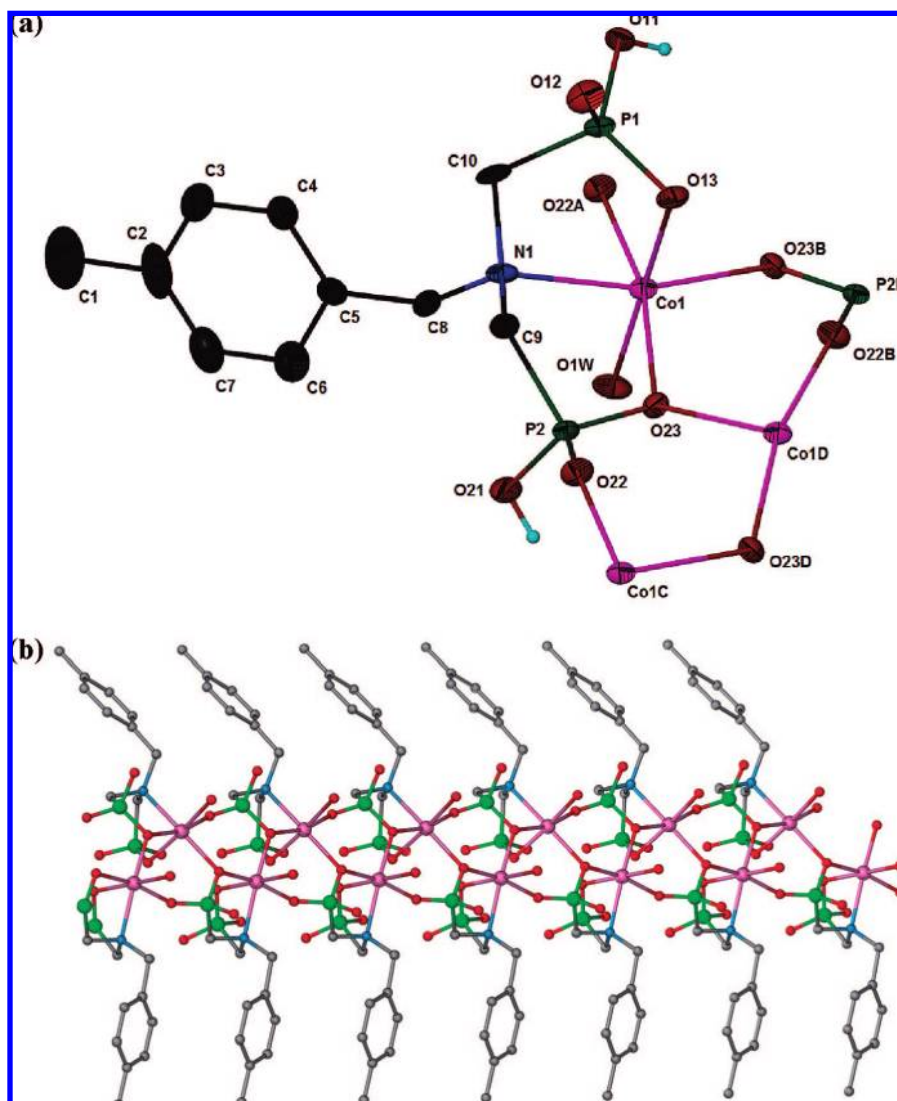
Figure 1. (a) ORTEP representation of the Co(H₂L)(H₂O) unit. The thermal ellipsoids are drawn at the 50% probability level. (b) Extension of the view in (a), looking down the c axis to emphasize the zigzag chain structure. The Co, P, N, and O atoms are shaded in pink, green, blue, and red, respectively.

because the corresponding ligand octahedra are rotated with respect to each other;[14] this situation results in spin canting. It should be pointed out, however, that the two cobalt centers in the chain are in identical environments of five oxygen atoms and one nitrogen atom.

The two lowest terms of a free Co(II) ion arising from the 3d⁷ configuration are the ⁴F ground term and the ⁴P term, which is separated from ⁴F by a gap of 15B, where B is the Racah parameter; the size of this gap is typically ~15,000 cm⁻¹. The octahedral ligand field splits the ⁴F atomic level into two orbital triplets, ⁴T₁ (ground) and ⁴T₂, and an orbital singlet ⁴A₂. The excited ⁴P state results in a ⁴T₁ term. In addition, the two ⁴T₁ terms are mixed by the cubic ligand field, so the ground state is mainly of ⁴F character but also contains an admixture of ⁴P. It should be mentioned that the one-electron orbitals in ⁴P and ⁴F in a crystal field (and also the crystal field parameter B) incorporate an admixture of the ligand orbitals (molecular orbitals). This is reflected by the introduction of orbital reduction factors into the model (see eq 4). The ground cubic ⁴T₁ term can be regarded as the state possessing an unquenched orbital angular momentum $l = 1$.

In regard to a fragment of the structure involving one Co(II) ion and its associated ligands (Figure 1), one can see that these surroundings can be approximately described by C_{4v} point-group

symmetry in which the tetragonal axis is expected to coincide with the N−Co−O axis in the distorted heteroligand coordination sphere. This situation dictates that along with spin−orbit coupling, the model should also include the tetragonal ligand fields acting on the Co(II) ions. First, let us assign the indices A and B to two Co(II) ions that occupy nonequivalent crystallographic positions in a 1D chain. Let us then introduce two local frames of reference related to ions A and B in the chain (Figure 4). The local Z_A and Z_B axes are chosen to coincide with the tetragonal axes, which subtend an angle φ. The Y_A and Y_B axes are chosen to be parallel to each other and perpendicular to the $Z_A Z_B$ plane, whereas the X_A and X_B axes lie in the $Z_A Z_B$ plane. It can be seen that the local axes for center B can be obtained from those related to center A by a turn through the angle φ around either the Y_A or Y_B axis. A tetragonal (axial) component of the ligand field splits the ground ⁴T₁ term of the Co(II) ion in C_{4v} symmetry into an orbital singlet ⁴A₂ and an orbital doublet ⁴E. The splitting of the cubic ⁴T₁ term by the axial ligand field and the spin−orbit interaction is described by the following single-ion Hamiltonian:[28,29]

$$\hat{H}_{Co}(p) = \Delta(\hat{l}_{Z_p}^2 - \tfrac{2}{3}) - \tfrac{3}{2}\kappa\lambda\hat{\mathbf{l}}\cdot\hat{\mathbf{s}}, \quad p = A, B \quad (4)$$

where $\hat{l}_{Z_p}$ are the operators for the projections of the orbital angular momentum onto the local Z axes, $\hat{\mathbf{l}}$ and $\hat{\mathbf{s}}$ are operators for the orbital

and spin angular momentum vectors, respectively, λ is the spin−orbit coupling parameter, which is negative for the Co(II) ion, and κ is the orbital reduction factor, which takes into account both the covalence effects and the mixing of the $^4T_1(^4F)$ and $^4T_1(^4P)$ terms by the cubic crystal field. The factor of $-^3/_2$ in eq 4 is conventionally introduced into the matrix of the angular momentum operator because of the fact that the matrix of $\hat{\mathbf{l}}$ within the $^4T_1(^4F)$ manifold coincides with the matrix of $-^3/_2\hat{\mathbf{l}}$ defined in the atomic (p) basis. The tetragonal field defined by the first term of eq 4 stabilizes the $^4A_2$ term (the state with $m_l = 0$) in the case of a positive tetragonal field ($\Delta > 0$) and the ^4E term (which has $m_l = \pm 1$) when $\Delta < 0$. The spin−orbit coupling produces further splitting of these levels into Kramers doublets.

Inspection of the geometry of the compound (Figure 1) shows that the tetragonal distortion of the heteroligand coordination environment of the Co(II) ion is quite strong. This observation allows us to assume that the tetragonal ligand field considerably exceeds the spin−orbit interaction (i.e., that $|\Delta| \gg \kappa|\lambda|$). The cases of positive and negative tetragonal field are different in essence, so the sign of Δ is crucial. In the strong positive-axial-field limit, the ground term $^4A_2$ is orbitally nondegenerate (conventionally, spin system), so the first-order orbital angular momentum is quenched. The second-order spin−orbit splitting of the ground tetragonal term $^4A_2$ can be described by the conventional zero-field-splitting Hamiltonian $D[\hat{s}_Z^2 - s(s + 1)/3]$, and in this case, the expected anisotropy would be relatively weak. It should be noted that in this case, the parameter D proves to be positive, which is incompatible with the observed SCM behavior. In addition, the experimental value of χT at room temperature indicates the presence of unquenched orbital angular momentum for the Co(II) ions in the $[Co(H_2L)(H_2O)]_\infty$ compound. Actually, the observed χT value of 3.2 emu K mol^{-1} at 300 K is higher than the value $\chi_{Co}T = 1.875$ emu K mol^{-1} expected for a spin system. Therefore, the spin formalism based on the second-order zero-field-splitting Hamiltonian seems to be irrelevant to the system under consideration, and a more general analysis based on the Hamiltonian given in eq 4 is required. There are some additional arguments in favor of the validity of the assumption that $\Delta < 0$. It has been shown[28] that the axial ligand field gives rise to magnetic anisotropy having an easy axis of magnetization when $\Delta < 0$ and an easy plane of magnetization when $\Delta > 0$. The $\Delta > 0$ case is incompatible with the observed SCM properties of the compound. In fact, the SCM behavior can be observed only in chains composed of magnetically coupled Ising spins (paramagnetic ions with easy axes of magnetization). This means that the case of positive axial field can be excluded from further consideration. Another argument in favor of the relevance of the case of $\Delta < 0$ is presented in the Results and Discussion. For this reason, we focus on the $\Delta < 0$ case, in which the axial ligand field stabilizes the orbital doublet ^4E.

Assuming that the splitting caused by the axial field significantly exceeds the spin−orbit splitting (i.e., the axial limit) and neglecting the spin−orbit mixing of the ^4E and $^4A_2$ terms, we arrive at the energy-level scheme shown in Figure 5. The spin−orbit interaction takes an axial form whose only nonvanishing component within the ground ^4E term is the Z component: $\hat{H}_{SO}^g(^4E) = -^3/_2\kappa\lambda\hat{l}_{Z_p}\hat{s}_{Z_p}$. This leads to the splitting of this term into four equidistant Kramers doublets, with the state based on $m_l = \pm 1$, $m_s = \mp^3/_2$ having the lowest energy. This is of course a simplification, but we will show that the experimental data can be perfectly explained within the model discussed thus far.

Along with the local frames, we will also use a molecular coordinate frame chosen in such a way that the molecular Z axis is directed along the bisector of the angle φ formed by the local Z_A and Z_B axes while the molecular Y axis is parallel to the local Y_A and Y_B axes (Figure 4).

The full Hamiltonian of the Co(II) pair includes the intracenter interactions described by eq 4 and the exchange interactions between the Co(II) ions. In general, the interaction between orbitally
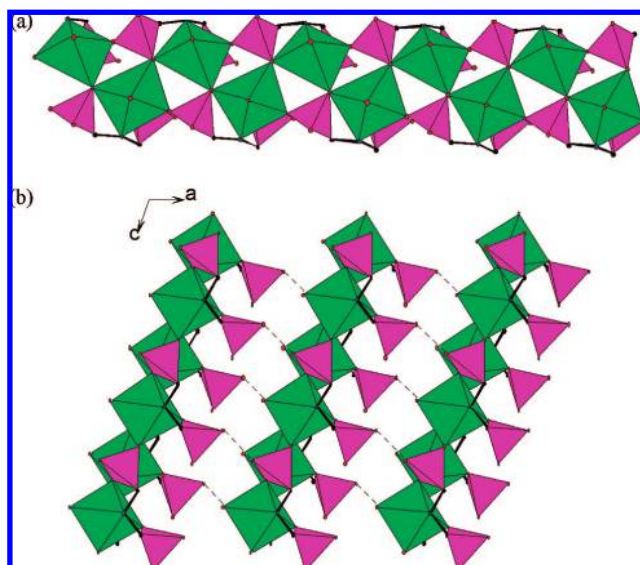

Figure 2. (a). A 1D zigzag chain of $[Co(H_2L)(H_2O)]_\infty$ viewed along the c axis. (b) A hydrogen-bonded metal phosphonate layer normal to the b axis. The 4-Me-C$_6$H$_4$-CH$_2$− groups of the diphosphonate ligands have been omitted for the sake of clarity. The cobalt octahedra and CPO$_3$ tetrahedra are shaded in green and pink, respectively. Hydrogen bonds are drawn as dotted lines.
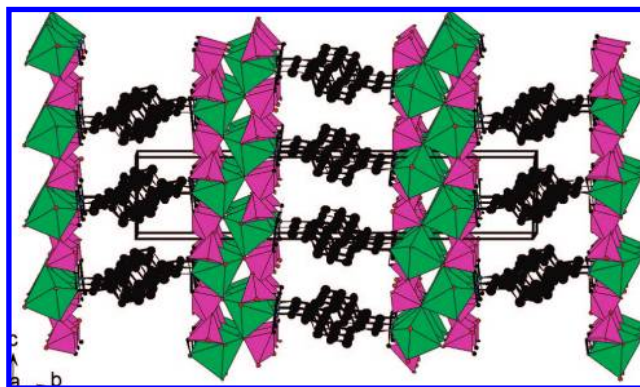

Figure 3. View of the structure of $[Co(H_2L)(H_2O)]_\infty$ down the a axis. The cobalt octahedra and CPO$_3$ tetrahedra are shaded in green and pink, respectively.
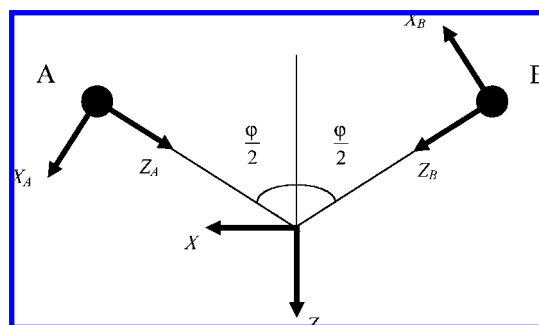

Figure 4. Local and molecular coordinates.

degenerate ions is described by the so-called orbitally dependent exchange Hamiltonian. Following the approximation proposed by

(28) Lines, M. E. *Phys. Rev.* **1963**, *131*, 546.
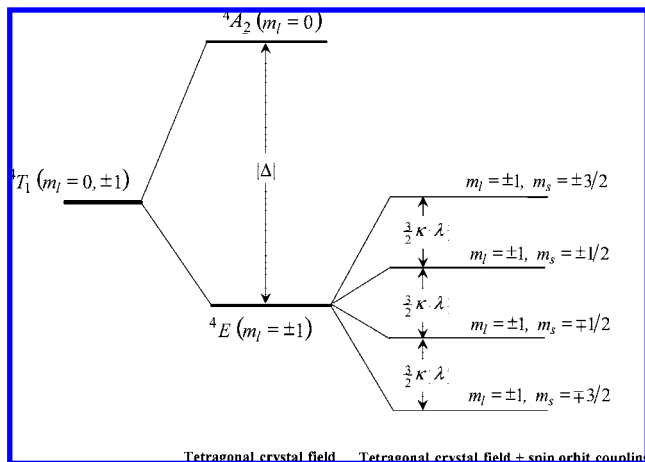(29) Lines, M. E. *J. Chem. Phys.* **1971**, *55*, 2977.

Figure 5. Splitting of the ground cubic $^4T_1(3d^7)$ term of the Co(II) ion by a tetragonal crystal field and spin−orbit coupling in the limit of a strong negative tetragonal field (neglecting spin−orbit mixing of the $^4A_2$ and ^4E terms).

Lines[28,29] and discussed in detail in our article[30] dealing with orbitally dependent superexchange between Co(II) ions, we assume that the exchange interaction can be described by the isotropic Heisenberg−Dirac−Van Vleck Hamiltonian

$$\hat{H}_{ex} = -2J\hat{s}_A \cdot \hat{s}_B = -2J[\hat{s}_X(A)\hat{s}_X(B) + \hat{s}_Y(A)\hat{s}_Y(B) + \hat{s}_Z(A)\hat{s}_Z(B)] \quad (5)$$

in which J is the exchange parameter and the single-ion spin operators $\hat{s}_A$ and $\hat{s}_B$ [with spins $s_A = s_B = {}^3/_2$ for the Co(II) ion] and the corresponding spin-projection operators $\hat{s}_\gamma(A)$ and $\hat{s}_\gamma(B)$ ($\gamma = X, Y, Z$) refer to the molecular frame. In the system under consideration, the exchange interaction is antiferromagnetic ($J < 0$). It is convenient to pass from the molecular-frame operators $\hat{s}_\gamma(A)$ and $\hat{s}_\gamma(B)$ to the operators $\hat{s}_{\gamma_A}$ and $\hat{s}_{\gamma_B}$ defined in the local frames. This transformation, which is performed with the aid of rotation matrices,[31] is given by eq SI.1 in the Supporting Information. When this is done, the exchange Hamiltonian in eq 5 becomes

$$\hat{H}_{ex} = -2J[\hat{s}_{Y_A}\hat{s}_{Y_B} + \cos(\varphi)(\hat{s}_{X_A}\hat{s}_{X_B} + \hat{s}_{Z_A}\hat{s}_{Z_B}) - \sin(\varphi)(\hat{s}_{X_A}\hat{s}_{Z_B} - \hat{s}_{Z_A}\hat{s}_{X_B})] \quad (6)$$

The Hamiltonian given by eq 6 is equivalent to the initial Hamiltonian (eq 5) and acts within the full basis set formed by the ground-state basis of the two Co(II) ions [i.e., the direct product of two $^4T_1$ bases (a 144 × 144 matrix)].

The energy gap between the ground Kramers doublet ($m_l = \pm 1$, $m_s = \mp {}^3/_2$) and the first excited one ($m_l = \pm 1, m_s = \mp {}^1/_2$) is assumed to exceed the exchange splitting, so at low temperatures we can restrict ourselves to considering only the ground Kramers doublet for each Co ion. All of the matrix elements of the operators $\hat{s}_{X_A}, \hat{s}_{Y_A}, \hat{s}_{X_B}$, and $\hat{s}_{Y_B}$ vanish within the basis set of the ground Kramers doublet:

$$\langle m_l = \pm 1, m_s = \mp {}^3/_2 | \hat{s}_{X_A} | m_l = \pm 1, m_s = \mp {}^3/_2 \rangle = 0$$
$$\langle m_l = \pm 1, m_s = \mp {}^3/_2 | \hat{s}_{X_A} | m_l = \mp 1, m_s = \pm {}^3/_2 \rangle = 0 \quad (7)$$

and so on. Hence, the Hamiltonian of eq 6 that deals with the "true" Co(II) spins ($s = {}^3/_2$) reduces to the Ising form for the pseudospins $s_{eff} = {}^1/_2$:[32]

(30) Palii, A. V.; Tsukerblat, B. S.; Coronado, E.; Clemente-Juan, J. M.; Borrás-Almenar, J. J. *J. Chem. Phys.* **2003**, *118*, 5566.
(31) Varshalovich, D. A.; Moskalev, A. N.; Khersonskii, V. K. *Quantum Theory of Angular Momentum*; World Scientific: Singapore, 1988.
(32) Palii, A. V. *Phys. Lett. A* **2007**, *365*, 116–121.

$$\hat{H}_{ex} = -2J_{eff}\hat{\tau}_{Z_A}\hat{\tau}_{Z_B} \quad (8)$$

where

$$J_{eff} = 9J\cos(\varphi) - \frac{3J^2\cos(\varphi)}{\kappa|\lambda|} \quad (9)$$

The term proportional to J^2 in eq 9 represents the second-order correction arising from mixing of the ground and excited manifolds of the cobalt pairs via the exchange interaction. One can see that the new exchange parameter reflects the geometry of the zigzag chain through the angle φ; meanwhile, in the adopted approximation it is independent of the axial crystal field. It is worth noting at this point that in the framework of the assumption adopted thus far, the effective exchange vanishes if the local axes are orthogonal ($\varphi = {}^\pi/_2$) and reaches the maximum value of ∼$9J$ in the linear geometry when the local axes coincide. This provides a possible recipe for chemical control of the magnetic properties of these types of 1D compounds. In the derivation of eq 8, we passed from the true spin-${}^3/_2$ operators $\hat{s}_{Z_A}$ and $\hat{s}_{Z_B}$ to the pseudospin-${}^1/_2$ operators $\hat{\tau}_{Z_A}$ and $\hat{\tau}_{Z_B}$. The pseudospin-${}^1/_2$ basis is chosen in such a way that the component of the ground Kramers doublet level with $m_l = -1$, $m_s = {}^3/_2$ ($m_l = 1, m_s = -{}^3/_2$) corresponds to the projection $\sigma = {}^1/_2$ ($\sigma = -{}^1/_2$) of the pseudospin ${}^1/_2$. With this choice for the correspondence between the effective and true bases, the effective single-ion pseudospin-${}^1/_2$ Hamiltonian in the presence of the external magnetic field is found to be[32]

$$\hat{H}_{Co}^{eff}(p) = g_\parallel\beta\hat{\tau}_{Z_p}H_{Z_p} - \Lambda_\perp(H_{X_p}{}^2 + H_{Y_p}{}^2), \quad p = A, B \quad (10)$$

where H_{X_p}, H_{Y_p}, and H_{Z_p} are the components of the magnetic field in the local frames and β is the Bohr magneton. The principal values of the effective **g** tensor for a Co(II) ion in its local surroundings are given by

$$g_\parallel = 3(\kappa + g_e) \quad \text{and} \quad g_\perp = 0 \quad (11)$$

where $g_\parallel$ is related to the local Z axes and $g_\perp$ to the local XY planes. One can see that the system is highly anisotropic in the ground state and that in particular, the first-order Zeeman splitting disappears in the perpendicular field. The values

$$\Lambda_\parallel = 0 \quad \text{and} \quad \Lambda_\perp = \frac{g_e{}^2\beta^2}{2\kappa|\lambda|} \quad (12)$$

are the principal values of the tensor of the Van Vleck temperature-independent paramagnetism (TIP). The TIP contribution appears as a result of Zeeman mixing of the ground Kramers doublet $|m_l = \pm 1, m_s = \mp 3/2\rangle$ with the three lowest excited states (Figure 5).

Using these results, we can write the following total Hamiltonian for a chain, including exchange and Zeeman terms:

$$\hat{H} = -2J_{eff}\sum_i \{[\hat{\tau}_{Z_A}(i)\hat{\tau}_{Z_B}(i) + \hat{\tau}_{Z_B}(i)\hat{\tau}_{Z_A}(i+1)] + g_\parallel\beta[\hat{\tau}_{Z_A}(i)H_{Z_A} + \hat{\tau}_{Z_B}(i)H_{Z_B}]\} \quad (13)$$

where the index i numbers the AB pairs. The TIP contribution will be added later.

In eq 13, both the pseudospin operators and the components of the magnetic field are defined in the local frames. To gain insight into the spin structure of the system, one can convert to the molecular frame with the aid of the relations given by eqs SI.2 and SI.3 in the Supporting Information. The exchange Hamiltonian then takes the form

$$\hat{H} = -2J_{eff}\sum_i \{\cos^2(\varphi/2)[\hat{\tau}_Z^A(i)\hat{\tau}_Z^B(i) + \hat{\tau}_Z^B(i)\hat{\tau}_Z^A(i+1)] - \sin^2(\varphi/2)$$
$$[\hat{\tau}_X^A(i)\hat{\tau}_X^B(i) + \hat{\tau}_X^B(i)\hat{\tau}_X^A(i+1)] - {}^1/_2\sin(\varphi)([\boldsymbol{\hat{\tau}}^A(i) \times \boldsymbol{\hat{\tau}}^B(i)]_Y +$$
$$[\boldsymbol{\hat{\tau}}^B(i) \times \boldsymbol{\hat{\tau}}^A(i+1)]_Y)\} + \beta[(g_{ZZ}^A\hat{\tau}_Z^A + g_{ZZ}^B\hat{\tau}_Z^B + g_{XZ}^A\hat{\tau}_X^A + g_{XZ}^B\hat{\tau}_X^B)H_Z +$$
$$(g_{XX}^A\hat{\tau}_X^A + g_{XX}^B\hat{\tau}_X^B + g_{ZX}^A\hat{\tau}_Z^A + g_{ZX}^B\hat{\tau}_Z^B)H_X] \quad (14)$$

where $\hat{\tau}_X^A(i)$, $\hat{\tau}_Z^A(i)$, $\hat{\tau}_X^B(i)$, $\hat{\tau}_Z^B(i)$, H_X, and H_Z are defined in the molecular frame, $\hat{\tau}_\gamma^p = \sum_i \hat{\tau}_\gamma^p(i)$ (p = A, B; γ = X, Z), and $[\hat{\tau}^A(i) \times \hat{\tau}^B(i)]$ is the vector product of the vector operators $\hat{\tau}^A(i)$ and $\hat{\tau}^B(i)$. Finally, the components of the **g** tensors are given by eq SI.4 in the Supporting Information.

One can see that after the isotropic exchange interactions between the "true" Co(II) spins have been projected onto the restricted space of the Kramers doublets, one arrives at the strongly anisotropic pseudo-spin-$^1/_2$ interaction given by eq 14, which produces a noncollinear spin structure. The first term in the sum over i in eq 14 describes an antiferromagnetic interaction with an effective parameter $J_{eff} \cos^2(\varphi/2)$ that tends to align the spins antiparallel in the Z direction. The second term describes a ferromagnetic interaction along the X axis with an effective parameter $-J_{eff} \sin^2(\varphi/2)$. This interaction is weaker than the antiferromagnetic coupling along the Z axis since $\varphi/2$ is less than $\pi/4$, but it plays an important role because it is responsible for the uncompensated magnetic moment of the chain. Finally, the last term in the sum involves the Y components of the vector products of the pseudo-spin operators and can be attributed to the antisymmetric Dzyaloshinsky–Moria exchange. The measure of this interaction is the effective antisymmetric exchange parameter $D_{AS} = J_{eff} \sin \varphi$. One can see that in the pseudo-spin Hamiltonian, the antisymmetric exchange is of the same order of magnitude as the remaining interactions, that is, it is not as small as in spin systems in which the orbital angular momenta are quenched.

Height of the Barrier and Magnetic Behavior of the Cochain. The formal similarity between the Hamiltonian given in eq 13 and the true Ising Hamiltonian (eq 1) provides a simple way to find the relation between the barrier height and the effective exchange parameter. Let us consider, for example, the single spin flip-flop process schematically depicted in Figure 6 (the spin of center B in an AB pair is overturned) in the absence of an external magnetic field. It follows from eq 13 that the energy loss in such a process is:

$$\Delta_b = E[\cdots\sigma_B(1) = \mp {}^1/_2 \cdots] - E[\cdots\sigma_B(1) = \pm {}^1/_2 \cdots] = 2|J_{eff}| \tag{15}$$

where only the spin projection $\sigma_B(1)$ is changed while the remaining ones keep their original values (all of the spin projections are defined in the local frames). We thus obtain the same relation as derived from the true Ising Hamiltonian (eq 3).

In order to calculate the magnetic susceptibility of the chain, it is convenient to present the total Hamiltonian of the chain in the presence of an external magnetic field applied along the molecular Z axis in the following form:

$$\hat{H}(\mathbf{H}\|Z) = -2J_{eff}\sum_i [\hat{\tau}_{Z_A}(i)\hat{\tau}_{Z_B}(i) + \hat{\tau}_{Z_B}(i)\hat{\tau}_{Z_A}(i+1)] +$$
$$g_\|\beta \cos(\varphi/2)H_Z\sum_i [\hat{\tau}_{Z_A}(i) + \hat{\tau}_{Z_B}(i)] \tag{16}$$

where the spin operators are defined in the local frames and the magnetic field is defined in the molecular frame. This Hamiltonian is of the Ising form, and therefore, one can use the analytical expression for the free energy (F) of the chain.[33] Adapting this expression to the case under consideration, we obtain

$$F(\mathbf{H}\|Z) = -Nk_BT \ln\left\{\exp\left(\frac{J_{eff}}{2k_BT}\right) \cosh\left[\frac{g_\|\beta \cos(\varphi/2)H_Z}{2k_BT}\right] + \sqrt{\exp\left(\frac{J_{eff}}{k_BT}\right)\sinh^2\left[\frac{g_\|\beta \cos(\varphi/2)H_Z}{2k_BT}\right] + \exp\left(-\frac{J_{eff}}{k_BT}\right)}\right\} \tag{17}$$

When the magnetic field is applied along the molecular X axis, the Hamiltonian of the system can be represented as

$$\hat{H}(\mathbf{H}\|X) = 2J_{eff}\sum_i [\hat{\tau}_{Z_A}(i)\hat{\tau}_{Z_B}'(i) + \hat{\tau}_{Z_B}'(i)\,\hat{\tau}_{Z_B}(i+1)] +$$
$$g_\|\beta \sin(\varphi/2)H_X\sum_i [\hat{\tau}_{Z_A}(i) + \hat{\tau}_{Z_B}'(i)] \tag{18}$$

where the operator $\hat{\tau}_{Z_B}'(i) \equiv -\hat{\tau}_{Z_B}(i)$ possesses the same eigenvalues as the operator $\hat{\tau}_{Z_B}(i)$. This Hamiltonian is also of the Ising form, and the free energy in the case of the magnetic field applied along the X axis is given by the expression

$$F(\mathbf{H}\|X) = -Nk_BT \ln\left\{\exp\left(-\frac{J_{eff}}{2k_BT}\right) \cosh\left[\frac{g_\|\beta \sin(\varphi/2)H_X}{2k_BT}\right] + \sqrt{\exp\left(-\frac{J_{eff}}{k_BT}\right)\sinh^2\left[\frac{g_\|\beta \sin(\varphi/2)H_X}{2k_BT}\right] + \exp\left(\frac{J_{eff}}{k_BT}\right)}\right\} \tag{19}$$

Using these expressions, one can calculate the principal values of the magnetic susceptibility tensor as

$$\chi_{ZZ} = -\frac{1}{H_Z}\frac{\partial}{\partial H_Z}F(\mathbf{H}\|Z), \quad \chi_{XX} = -\frac{1}{H_X}\frac{\partial}{\partial H_X}F(\mathbf{H}\|X), \quad \chi_{YY} = 0 \tag{20}$$

The average magnetic susceptibility is calculated as $\bar{\chi} = (\chi_{ZZ} + \chi_{XX})/3$. This expression should be supplemented by a TIP contribution. The latter can be calculated with the aid of the pseudospin-$^1/_2$ Hamiltonian for a single Co(II) ion (eq 10). We find that the TIP tensor components $\chi_\|^{TIP}$ and $\chi_\perp^{TIP}$ and the average TIP contribution $\bar{\chi}^{TIP}$ for the Co(II) ion are given by[32]

$$\chi_\|^{TIP} = 0, \quad \chi_\perp^{TIP} = \frac{Ng_e^2\beta^2}{\kappa|\lambda|}, \quad \bar{\chi}^{TIP} = \frac{2Ng_e^2\beta^2}{3\kappa|\lambda|} \tag{21}$$

where the symbols $\|$ and $\perp$ are related to the local frames.

Results and Discussion

The temperature dependence of the relaxation time for the $[Co(H_2L)(H_2O)]_\infty$ compound was obtained from the frequency dependence of the in-phase ($\{\chi'\}$) and out-of-phase ($\{\chi''\}$) ac susceptibility data.[14] These data are shown in Figure 7. The experimental data for τ obtained in this manner (see ref 14 for more details) were fit to the Arrhenius expression (eq 2) presented in the form

$$\ln\left(\frac{1}{\tau}\right) = -\frac{\Delta_b}{k_BT} - \ln(\tau_0) \tag{22}$$

The experimental and calculated plots of $\ln(1/\tau)$ versus $1/T$ are shown in Figure 8. The best-fit parameters were found to be $\Delta_b(\chi') = 18.6$ cm^{-1} and $\tau_0(\chi') = 3.4 \times 10^{-9}$ s for the in-phase frequency-scan signal and $\Delta_b(\chi'') = 20.2$ cm^{-1} and $\tau_0(\chi'') = 8.4 \times 10^{-10}$ s for the out-of-phase signal. Then, considering the simple average $[\Delta_b(\chi') + \Delta_b(\chi'')]/2 = 19.4$ cm^{-1} as a reasonable value for the barrier height Δ_b, one can deduce from eq 15 that $J_{eff} = -9.7$ cm^{-1}.

Magnetic susceptibility measurements performed on a polycrystalline sample of the compound at $H = 0.1$ T over the temperature range 2−50 K revealed the behavior shown in Figure 9, which is quite similar to that observed in ferrimagnetic spin chains.[34] As the temperature was decreased, the χT value decreased and reached a minimum of 0.6 emu K mol^{-1} at 7 K. Below 7 K, χT increased abruptly, reached a maximum at ∼2.5 K ($\chi T_{max} = 2.5$ emu K mol^{-1}), and finally decreased again at lower temperatures. The observed increase of χT below 7 K can be attributed to the fact that antiferromagnetic coupling does not lead to the exact cancellation of the magnetic moments as

(33) Yeomans, J. M. *Statistical Mechanics of Phase Transitions*; Clarendon Press: Oxford, U.K., 1992.

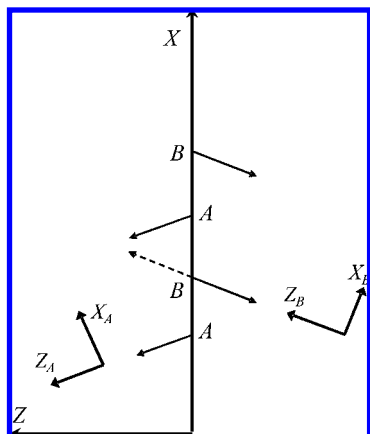(34) Kahn, O. *Molecular Magnetism*; VCH Publishers: New York, 1993.

Figure 6. Noncollinear spin structure of the chain and illustration for a single spin flip-flop process.
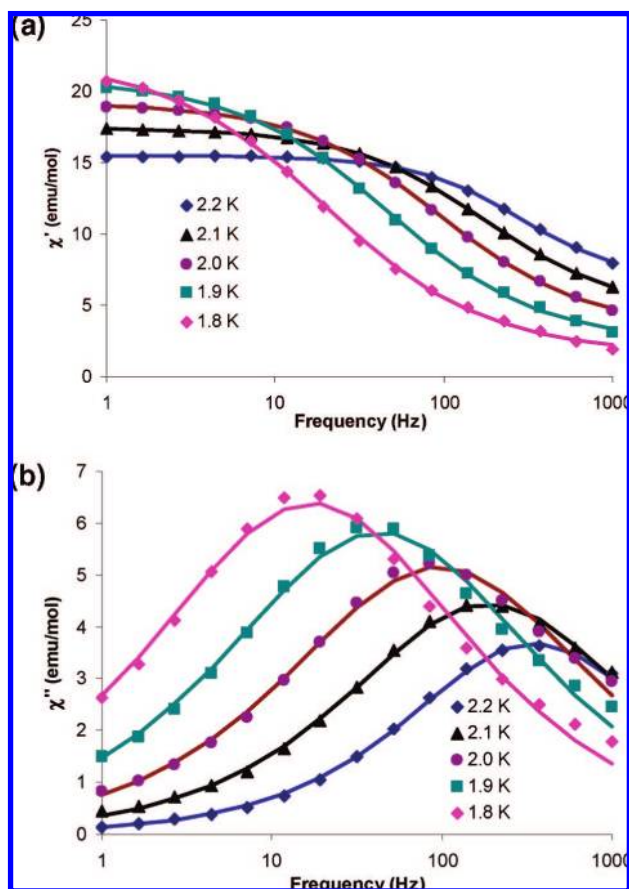

Figure 7. Frequency dependence of the (top) χ' and (bottom) χ'' components of the ac magnetic susceptibility of $[Co(H_2L)(H_2O)]_\infty$ measured in an oscillating field of 3 Oe at various temperatures. The solid lines are merely guides for the eye.
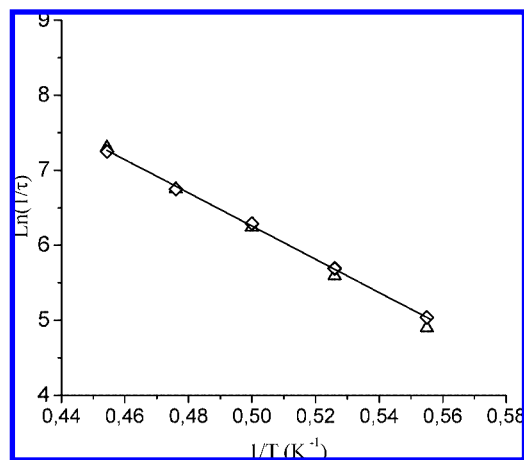

Figure 8. Temperature dependence of the relaxation time. The triangles and diamonds represent the relaxation times obtained from frequency dependence of χ' and χ'', respectively. The solid line corresponds to the best fit of the data to eq 22.
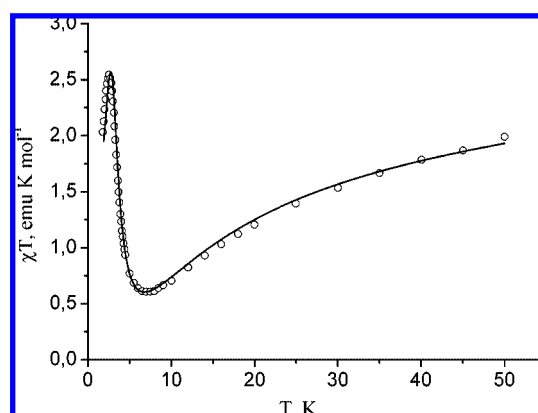

Figure 9. Temperature dependence of χT for $[Co(H_2L)(H_2O)]_\infty$. Circles represent the experimental data reported in ref 18, and the solid line is the theoretical curve calculated using the parameter values $\lambda = -180$ cm^{-1}, $\kappa = 0.8$, $J_{\text{eff}} = -9.7$ cm^{-1}, and $\varphi = 15°$.

can be explained by the presence of the lower-symmetry crystal field in the Co surroundings, which leads to a deviation of the magnetic axes from the geometrical ones. At the same time, we have employed a simplified model dealing with the limiting case of strong tetragonal field, which can also give an error in the estimation of the angle. Figure 9 shows an essentially perfect agreement between the observed and calculated χT-versus-T curves, thus indicating that the theory presented here adequately describes simultaneously both the dynamic and static magnetic properties of the compound.

Figure 10 displays $\chi_{ZZ}T$-versus-T and $\chi_{XX}T$-versus-T curves calculated using the parameter values $\lambda = -180$ cm^{-1}, $\kappa = 0.8$, $J_{\text{eff}} = -9.7$ cm^{-1}, and $\varphi = 15°$. These plots demonstrate that the magnetic moments along the Z axis are fully canceled at low temperatures but an uncompensated magnetic moment appears along the X axis, resulting in the distinct maximum in the $\chi_{XX}T$-versus-T curve.

Earlier we presented a preliminary argument in favor of a negative sign for the axial field. We now provide additional justification for this assumption and demonstrate that the appearance of the uncompensated magnetic moment along the X axis cannot be explained if it is assumed that Δ is positive. Figure 11 shows that for $\Delta > 0$, the easy planes of magnetization for the ions A and B coincide with the local X_pY_p ($p = A, B$)
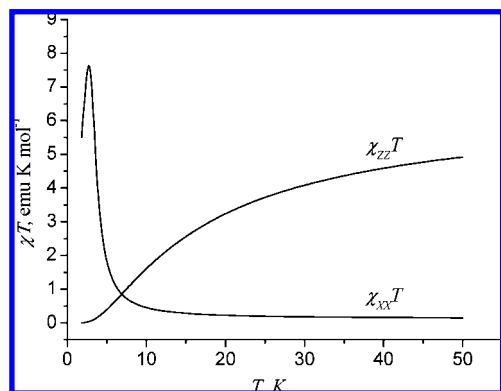
a result of spin canting. In the calculation of χT, we used the values $\lambda = -180$ cm^{-1} and $\kappa = 0.8$, which are typical for the high-spin Co(II) ion, and the effective exchange parameter value $J_{\text{eff}} = -9.7$ cm^{-1} obtained from the Arrhenius plot. Since the directions of the magnetic anisotropy axes can be different from those of the local C_4 axes, the canting angle φ was allowed to vary in the course of fitting the experimental χT-versus-T curve. The best fit was achieved for the angle $\varphi = 15°$. The significant difference of the angle obtained from the geometry of the structure and the angle between the local magnetic axes

Figure 10. Temperature dependence of the nonzero diagonal components of the χT tensor calculated using the parameter values $\lambda = -180$ cm^{-1}, $\kappa = 0.8$, $J_{eff} = -9.7$ cm^{-1}, and $\varphi = 15°$.
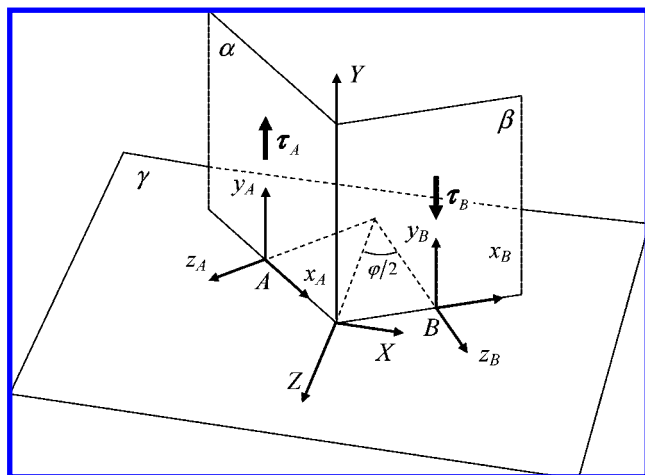

Figure 11. Illustration of the full cancellation of the magnetic moments of ions A and B in the case of a positive axial crystal field.

Figure 12. Exchange parameters $J_{\alpha_A\gamma_B}$ as functions of Δ calculated using the parameter values $J = -1.1$ cm^{-1}, $\lambda = -180$ cm^{-1}, $\kappa = 0.8$, and $\varphi = 15°$.

Figure 13. Principal values of the **g** tensor as functions of Δ calculated using the parameter values $J = -1.1$ cm^{-1}, $\lambda = -180$ cm^{-1}, $\kappa = 0.8$, and $\varphi = 15°$.

planes (these planes are assigned as planes α and β for centers A and B, respectively). In the absence of the exchange interaction between Co(II) ions, all of the orientations of the spins $\boldsymbol{\tau}_A$ and $\boldsymbol{\tau}_B$ within the corresponding easy planes are energetically equivalent. In the presence of the antiferromagnetic exchange between the Co ions, these orientations become inequivalent, since the exchange interaction tends to orient the interacting spins antiparallel. There is a unique possibility of minimizing both the single-ion and exchange energies: aligning the spins $\boldsymbol{\tau}_A$ and $\boldsymbol{\tau}_B$ antiparallel along the line where the α and β planes cross (the molecular Y axis). As a consequence, the magnetic moments of ions A and B cancel each other, and the total magnetic moment vanishes. On the contrary, in the case of negative Δ, at low temperatures the spins $\boldsymbol{\tau}_A$ and $\boldsymbol{\tau}_B$ tend to align along the local easy axes of magnetization, provided that the local anisotropy is strong enough to avoid being suppressed by the exchange interaction. These easy axes for the neighboring ions are not parallel, and the resulting nonzero magnetic moment appears along the molecular X axis as a result of the spin-canting effect (Figure 6). Therefore, we arrive at the conclusion that our initial assumption of a negative sign for the axial field parameter is the only way to explain the magnetic behavior of the Co(H$_2$L)(H$_2$O) compound.

The approach proposed in this article is essentially based on the assumption that the condition $|\Delta| \gg \kappa|\lambda| \gg |J|$ is fulfilled and hence that the system is close to the axial limit, for which
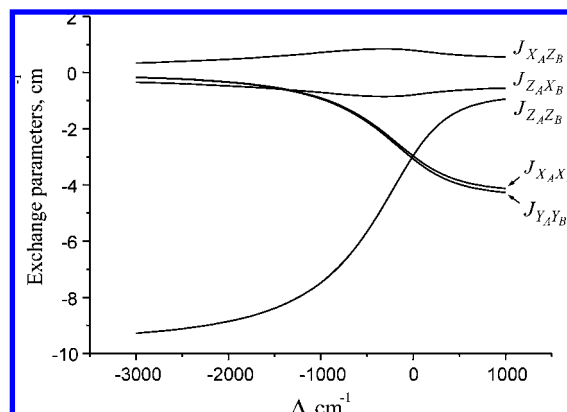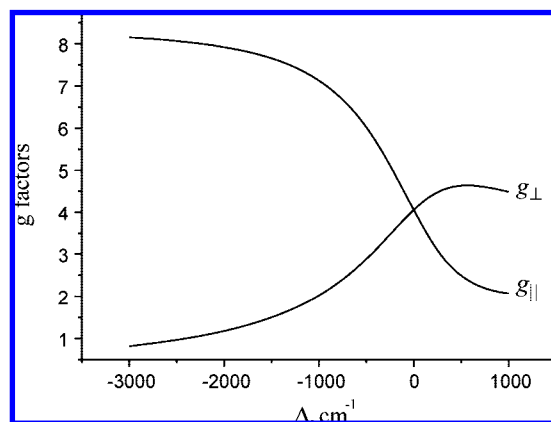
the effective Hamiltonian defined in the local frames is expressed in terms of the operators for the pseudospin-$^1/_2$ Z components (eq 13). Therefore, it is reasonable to estimate a possible range for the values of the axial field parameter Δ for which the exchange Hamiltonian is close to the Ising form and $g_\perp$ becomes negligible compared with $g_\parallel$. In order to find the dependence of the effective Hamiltonian parameters on the parameters Δ and J, we can use the approach developed in our earlier paper.[18] The general form of the exchange Hamiltonian for the AB cobalt pair is the following:

$$\hat{H}(A, B) = -2 \sum_{\alpha,\gamma=X,Y,Z} J_{\alpha_A\gamma_B}\hat{\tau}_{\alpha_A}\hat{\tau}_{\gamma_B} + \beta \sum_{p=A,B} [g_\parallel\hat{\tau}_{Z_p}H_{Z_p} + g_\perp(\hat{\tau}_{X_p}H_{X_p} + \hat{\tau}_{Y_p}H_{Y_p})] \quad (23)$$

It follows from eq 9 that the exchange integral J corresponding to $J_{eff} = -9.7$ cm^{-1} and $\varphi = 15°$ is $J \approx -1.1$ cm^{-1}. Figures 12 and 13 show the nonzero exchange parameters $J_{\alpha_A\gamma_B}$ and the principal values of **g** tensor, respectively, as functions of Δ calculated using the parameter values $J = -1.1$ cm^{-1}, $\lambda = -180$ cm^{-1}, $\kappa = 0.8$, and $\varphi = 15°$. One can see that all of the exchange parameters $J_{\alpha_A\gamma_B}$ except for $J_{Z_AZ_B}$ are vanishing for $\Delta < 0$ and $|\Delta| \geq 1500$ cm^{-1} and also that $g_\parallel \gg g_\perp$ in this range of Δ values. It should be noted that the **g** tensor tends to its axial limit more slowly than the exchange tensor. Values of the axial crystal field parameter falling in the range 1500 cm^{-1} $\leq |\Delta| \leq 2000$ cm^{-1} are realistic for transition-metal ions in an

axially distorted ligand environment. This means that the adopted approximation is well-justified for reasonable values of the axial crystal field parameters and thus can be successfully used for the description of SCM behavior of spin-canted chains based on Co(II) ions.

Concluding Remarks. The quantum-mechanical approach described in this work represents the first attempt to explain by theory the SCM behavior and spin-canting phenomenon in the zigzag-chain compound $[Co(H_2L)(H_2O)]_\infty$ $[L = 4\text{-Me-}C_6H_4\text{-}CH_2N(CPO_3H_2)_2]$, which are based on the fact that the antiferromagnetically coupled Co(II) ions possess unquenched orbital angular momenta. The model we have elaborated takes into account the strong axial crystal fields acting on the Co(II) ions, the spin−orbit interaction, antiferromagnetic exchange, and the zigzag structure of the chain. The deduced pseudospin-$^1/_2$ Hamiltonian contains ferro- and antiferromagnetic contributions as well as a contribution that can be attributed to antisymmetric exchange. The combination of these factors gives rise to a canted spin structure and subsequently to an uncompensated magnetic moment. The proposed model provides a reasonable explanation of the observed static (temperature dependence of the dc magnetic susceptibility) and dynamic (frequency dependence of the in-phase and out-of-phase ac susceptibilities) magnetic properties of the chain. Therefore, one can conclude that in spite of the fact that the model is relatively simple, it adequately incorporates the main factors governing the SCM behavior of the compound.

Two more points should also be emphasized. First, the developed model is applicable not only to the spin-canted Co(II) chains but also to chains composed of other Kramers ions. Second, the model is not restricted to the case of antiferromagnetic exchange. In fact, the key expressions (eqs 17 and 19) are valid for both ferro- and antiferromagnetic spin-canted chains.

We also wish to point out that we neglected the vibronic coupling in this model, resulting in the $^4E \otimes (b_1 + b_2)$ Jahn−Teller problem for the ground orbital doublet ^4E of the Co(II) ion. In general, the Jahn−Teller coupling removes the orbital degeneracy (in classical terms) and consequently reduces the orbital magnetic contribution. To some extent, this is taken into account by the reduction factors. In a more general sense (especially when the vibronic coupling is moderate), a solution of the dynamical Jahn−Teller problem is required. These results will be published in due course.

Supporting Information Available: Relations between the pseudo-spin-$^1/_2$ operators and magnetic field components defined in local and molecular frames, expressions for the components of the local **g** tensors defined in the molecular frame, and a CIF file for $[Co(H_2L)(H_2O)]_\infty$. This material is available free of charge via the Internet at http://pubs.acs.org.

JA8050052